Subtractive Non-Contrast-Enhanced Magnetic Resonance Imaging of Lower Limb Veins using Multiple Flow-Dependent Preparation Strategies

Authors:

Hao Li,[1]* Andrew N Priest,[2]* Ilse Patterson,[2] Martin J Graves,[2] David J Lomas[1]

[1]Department of Radiology, University of Cambridge, Cambridge, United Kingdom.

[2]Department of Radiology, Addenbrooke's Hospital, Cambridge, United Kingdom.

* H. Li and A. N. Priest contributed equally to this work and jointly share first authorship.

Word count (body of text): 4978

Figure and table number: 10

Running head: NCE-MRV Using Multiple Flow-Dependent Preparations

ABSTRACT

Purpose:

To evaluate the performance of Acceleration-Dependent Vascular Anatomy for Non-Contrast-Enhanced MR Venography (ADVANCE-MRV) in femoral veins and investigate whether venous signal uniformity can be improved by applying multiple acquisitions with different flow-suppressions or multiple flow-suppressions in one acquisition.

Method:

ADVANCE-MRV uses flow-sensitised modules to acquire a dark-artery image set and a dark-artery-vein set, which are subsequently subtracted. Ten healthy volunteers were imaged, using the ADVANCE-MRV sequence with improved venous suppression uniformity in the dark-artery-vein images achieved by applying multiple flow-suppressions in the same acquisition or by combining multiple images acquired with different flow-suppressions. The performance of the improved technique was also evaluated in thirteen patients with lower-limb deep venous thrombosis (DVT).

Results:

Multiple-preparation and multiple-acquisition approaches all improved venous signal uniformity and reduced the signal void artefacts observed in the original ADVANCE-MRV images. The multiple-acquisition approaches achieved excellent blood signal uniformity and intensity, albeit at the cost of an increase in the total acquisition time. The double-preparation approach demonstrated good performance in all measurements, providing a good compromise between signal uniformity and acquisition time. The blood signal spatial variation and its variation using different gradient amplitudes were reduced by 20% and 29%. All patient images showed uniform and bright venous signal in non-occluded sections of vein.

Conclusion:

The enhanced ADVANCE-MRV methods substantially improved signal uniformity in healthy volunteers and patients with known DVT. The double-preparation approach gave good quality femoral vein images providing improved venous signal uniformity without increasing acquisition time in comparison to the original sequence.

Keywords:

MR venography; non-contrast enhanced; venous thrombosis

INTRODUCTION

Lower limb deep venous thrombosis (DVT) is a common disease with potentially fatal complications, such as pulmonary embolism. Thromboses often start in the deep veins of the leg, from where they may extend to proximal veins, and subsequently break free to cause a pulmonary embolism (1). The initial development of a DVT can be clinically asymptomatic (2), and the accurate diagnosis of DVT is important for its treatment and the prevention of complications.

Ultrasonography is widely considered as a primary diagnostic procedure for the initial assessment of symptomatic DVT (1). However, an ultrasound examination can be difficult or limited in many cases, such as in patients with marked obesity, swollen extremities or overlying casts, and after orthopaedic surgery (2–4). Conventional X-ray venography is still considered as the diagnostic reference standard but is infrequently performed as it requires the intravenous injection of an iodinated contrast media and exposure to ionising radiation. Computed tomographic (CT) venography, in combination with pulmonary CT angiography, is an alternative technique to identify venous thromboses, but is primarily used for patients with suspected pulmonary embolism (5). However, it also involves exposure to ionising radiation and the use of potentially nephrotoxic contrast media.

MRI techniques have been proposed and gained increasing popularity in the diagnosis of DVT. For example, MR direct thrombus imaging (MR-DTI) (6) can be used to directly visualise acute thrombus. Dark-blood approaches such as T1-weighted 3D variable flip-angle turbo-spin-echo (SPACE) (7,8) and DANTE-SPACE (9) were reported to allow direct visualisation of non-acute DVT within the dark venous lumen. MR venography (MRV) is another effective technique, which can visualise the peripheral venous system and diagnose DVT by detecting the filling defects within the lumen or the absence of flow signal. Moreover, MRV can also be combined with MR-DTI to assess thrombus age in cases of suspected recurrence (10,11).

Current MRV techniques mainly use a gadolinium-based contrast agent (GBCA). In practice, these agents are less effective for venography than arteriography owing to tissue redistribution. They are also challenging to use: acquisition timing can be difficult, and venous enhancement may be unpredictable and inadequate for diagnostic purposes. Additionally, GBCAs have raised concerns, firstly over the development of nephrogenic systemic fibrosis in renal failure patients (12), and more recently over long-term retention of gadolinium in the brain and other tissues (13–15). This has led to warning notices by the FDA (16) and the suspension of several linear gadolinium contrast agents by the European Medicines Agency (17). Such concerns have further increased interest in developing exogenous contrast-free alternative methods.

As the earliest non-contrast-enhanced MRV (NCE-MRV) technique, two-dimensional (2D) time-of-flight (TOF) (18) reported promising results but is limited by acquisition plane and is prone to motion and flow artefacts (19). Balanced steady-state free precession (bSSFP) can be used to yield bright venous blood images with a high signal-to-noise ratio (20). However, the high signal intensity of background issue, including the arterial signal, masks the veins when creating a projection angiogram. Recently, a new technique using velocity-selective magnetisation preparation and transient bSSFP was demonstrated to generate high-contrast venograms, but it may be sensitive to the velocity of flow and lacks validation in DVT patients (21).

Some methods, based on multiple acquisitions and image subtraction, have been proposed to generate vein-only images, such as the technique using both flow-refocused fresh-blood imaging (FR-FBI) and swap phase-encode arterial double-subtraction elimination (SPADE) (22). Another multi-acquisition approach is to use motion-sensitised preparation modules to suppress signals from flowing blood, due to intra-voxel velocity dispersion (23-26). These methods can achieve complete separation between arteries and veins and excellent background tissue suppression.

However, motion-sensitised preparation approaches rely on dispersion of the blood flow velocities within each imaging voxel, to achieve good signal suppression. For venous blood especially, such intra-voxel dispersion can be weak. Consequently, blood-suppression efficiency may be reduced, so that luminal image quality is impaired by apparent signal void artefacts in the subtracted angiograms (27). We have reported two strategies that can solve this problem in previous conference presentations. One approach is to acquire several datasets with different first-order gradient moments, and then to take the minimum signal (27). Another approach is to apply multiple flow-suppression modules in one acquisition (28).

In this article, Acceleration-Dependent Vascular Anatomy for Non-Contrast-Enhanced MR Venography (ADVANCE-MRV) is firstly described as a new NCE-MRV technique. Then, the impact of flow dispersion on venous signals is evaluated. After that, the two strategies, multiple-acquisition and multiple-preparation, are developed and optimized to solve the signal-void problem and achieve bright uniform venous signal. The performances of the two methods are finally compared with the original ADVANCE-MRV technique.

THEORY

Sequence design of ADVANCE-MRV

ADVANCE-MRV employs two different preparation modules to acquire two co-located image sets, one with the arterial signal suppressed (the 'dark-artery' images) and the other with both arterial and venous signals suppressed (the 'dark-artery-vein' images). Then the two sets are subtracted to give an angiogram featuring the veins only (Fig. 1). Fig. 2 shows the schematic diagram of the pulse sequence. ADVANCE-MRV consists of a blood-suppression preparation module, a delay time (TD), two spectral fat suppression modules (27) and a 3D segmented bSSFP readout sequence, preceded by 10 dummy excitations with sinusoidally increasing amplitudes (Fig. 2c).

The dark-vein-artery images are acquired by using an improved motion-sensitised driven-equilibrium (iMSDE) module (29), which is a velocity-sensitive preparation module to suppress both venous and arterial signal (Fig. 2a). The velocity-encoding parameter ***venc*** is determined by the effective first gradient moment ($\mathbf{m_1}$) of the gradient waveforms. For the dark-artery images, an acceleration-sensitised module (24) is employed to suppress the arterial signal only (Fig. 2b). This sequence has an effective first gradient moment of zero, so has no sensitisation to the constant-velocity flow which normally occurs in the peripheral veins. Its acceleration-encoding parameter ***aenc*** is determined by its effective second gradient moment ($\mathbf{m_2}$). Both the velocity- and acceleration-sensitised preparation modules use composite refocusing and tip-up pulses (23), and the duration of a 90° pulse is 0.4 ms. Timing parameters (defined in Fig. 2) were δ = 4 ms, Δ = 6.8–7.5 ms, τ = 12.5–13.8 ms.

Signal attenuation introduced by the iMSDE preparation module

In the dark-vein images, the signal attenuation introduced by the velocity-sensitive iMSDE module depends partly on the mean velocity within each voxel, and partly on the variation (dispersion) of velocity within the voxel.

Assuming a uniform spin density $\rho_0(\mathbf{r}_0)$ over a given voxel centred at $\mathbf{r}_0(x_0, y_0, z_0)$, after the first $90°_{+x}$ pulse, the transverse magnetisation of the voxel can be expressed as

$$M_{xy0}(\mathbf{r}_0) = \iiint_{voxel} \rho_0(\mathbf{r}_0)\ \mathrm{d}^3\mathbf{r} = \Delta V \rho_0(\mathbf{r}_0) \tag{1}$$

where ΔV is the volume of a voxel.

Now assuming the voxel contains a spread of constant velocity spins, after experiencing the gradients in the preparation module, the transverse magnetisation is

$$M_{xy}(\mathbf{r}_0) = \iiint_{voxel} \rho_0(\mathbf{r}_0)\, e^{i\phi(\mathbf{r})}\, \mathrm{d}^3\mathbf{r} = \iiint_{voxel} \rho_0(\mathbf{r})\, e^{-i\gamma \mathbf{m_1}\cdot\mathbf{v}(\mathbf{r})}\, \mathrm{d}^3\mathbf{r} \tag{2}$$

where $\phi(\mathbf{r})$ is the phase shift during the preparation module, which is given by $\phi(\mathbf{r}) = -\gamma \mathbf{m_1} \cdot \mathbf{v}(\mathbf{r})$ (30), $\mathbf{m_1}$ is the first gradient moment of the preparation module.

If the voxel is small enough, the velocity variation can be considered as approximately linear over the voxel,

$$\mathbf{v}(\mathbf{r}) = \mathbf{v}(\mathbf{r_0}) + \nabla \mathbf{v}(\mathbf{r_0}) \cdot (\mathbf{r} - \mathbf{r_0}) \tag{3}$$

Then,

$$\begin{aligned} M_{xy}(\mathbf{r}_0) &= \iiint_{voxel} \rho_0(\mathbf{r}_0) e^{-i\gamma \mathbf{m_1} \cdot \mathbf{v}(\mathbf{r_0})} e^{-i\gamma \mathbf{m_1} \cdot \nabla \mathbf{v}(\mathbf{r_0}) \cdot (\mathbf{r} - \mathbf{r_0})} \, \mathrm{d}^3 \mathbf{r} \\ &= M_{z0}(\mathbf{r}_0) e^{-i\gamma \mathbf{m_1} \cdot \mathbf{v}(\mathbf{r_0})} \operatorname{sinc}(\boldsymbol{\beta}_\mathbf{x} \cdot \mathbf{m_1} \Delta x) \operatorname{sinc}(\boldsymbol{\beta}_\mathbf{y} \cdot \mathbf{m_1} \Delta y) \operatorname{sinc}(\boldsymbol{\beta}_\mathbf{z} \cdot \mathbf{m_1} \Delta z) \end{aligned} \tag{4}$$

where $\boldsymbol{\beta}_\mathbf{x} = \frac{\gamma}{2} \cdot \frac{\partial \mathbf{v}(\mathbf{r_0})}{\partial x}$, $\boldsymbol{\beta}_\mathbf{y} = \frac{\gamma}{2} \cdot \frac{\partial \mathbf{v}(\mathbf{r_0})}{\partial y}$, $\boldsymbol{\beta}_\mathbf{z} = \frac{\gamma}{2} \cdot \frac{\partial \mathbf{v}(\mathbf{r_0})}{\partial z}$, Δx, Δy and Δz are the sizes of the voxel.

After the final 90°$_{-x}$ pulse, the magnetisation component along the y-direction will be rotated back to the z-axis, while the component along the x-direction will stay in the transverse plane. Therefore, longitudinal magnetisation after the pulse only contains the real component of the transverse magnetisation:

$$\begin{aligned} M_z(\mathbf{r}_0) &= \mathrm{Real}\left(M_{z0}(\mathbf{r}_0) e^{-i\gamma \mathbf{m_1} \cdot \mathbf{v}(\mathbf{r_0})} \operatorname{sinc}(\boldsymbol{\beta}_\mathbf{x} \cdot \mathbf{m_1} \Delta x) \operatorname{sinc}(\boldsymbol{\beta}_\mathbf{y} \cdot \mathbf{m_1} \Delta y) \operatorname{sinc}(\boldsymbol{\beta}_\mathbf{z} \cdot \mathbf{m_1} \Delta z) \right) \\ &= M_{z0}(\mathbf{r}_0) \cos(\gamma \mathbf{m_1} \cdot \mathbf{v}(\mathbf{r_0})) \operatorname{sinc}(\boldsymbol{\beta}_\mathbf{x} \cdot \mathbf{m_1} \Delta x) \operatorname{sinc}(\boldsymbol{\beta}_\mathbf{y} \cdot \mathbf{m_1} \Delta y) \operatorname{sinc}(\boldsymbol{\beta}_\mathbf{z} \cdot \mathbf{m_1} \Delta z) \end{aligned} \tag{5}$$

Therefore, the signal attenuation of the voxel during the iMSDE preparation module is

$$\eta(\mathbf{r}_0) = \cos(\gamma \mathbf{m_1} \cdot \mathbf{v}(\mathbf{r_0})) \operatorname{sinc}(\boldsymbol{\beta}_\mathbf{x} \cdot \mathbf{m_1} \Delta x) \operatorname{sinc}(\boldsymbol{\beta}_\mathbf{y} \cdot \mathbf{m_1} \Delta y) \operatorname{sinc}(\boldsymbol{\beta}_\mathbf{z} \cdot \mathbf{m_1} \Delta z) \tag{6}$$

The expression for the signal in equation (6) contains two components. The decaying component, given by the sinc function, is related to the variation of the velocity within the voxel. The function $\cos(\phi(x_0, y_0))$ refers to an oscillatory component that reflects the average velocity, which could be highly relevant in voxels with little velocity dispersion.

Strategies using multiple acquisitions and multiple preparations

As demonstrated by the above analysis, for cases with very low intra-voxel velocity dispersion, the signal will not be reliably suppressed but is, instead, an oscillatory function of the mean velocity. Thus, a single velocity-sensitive iMSDE module cannot be relied upon to completely suppress the vascular signals. Two

strategies, multiple-acquisition and multiple-preparation, are developed to try and solve the signal oscillation problem. The multiple-acquisition method acquires several velocity-sensitised datasets with the first gradient moment of the preparation module decreasing by successive factors of two each time. By taking the minimum signal of the datasets, the potential signal oscillation will be removed, and the venous signal will be maintained at a small value. However, the multiple-acquisition method increases the total scan time. An alternative strategy is to apply multiple flow-suppression modules in one acquisition. By combining two or three sequential velocity-sensitised preparation modules before the image readout and decreasing the first gradient moment by successive factors of two, reasonable flow-suppression should be achieved over a range of velocities, even in regions with very low velocity dispersion. The same number of additional T_2 preparation modules without gradients were also applied for the acceleration-sensitised acquisition to ensure that the static tissue signal undergoes the same potential decay.

Signal attenuation simulation for the two strategies

The signal attenuation functions of multiple-acquisition and multiple-preparation modules are

$$\eta_{multi\text{-}acq} = \min\left(\eta_{single_1}, \eta_{single_2}, \eta_{single_3}, \cdots, \eta_{single_n}\right) \tag{7}$$

$$\eta_{multi-prep} = \eta_{single_1}\eta_{single_2}\eta_{single_3}\cdots\eta_{single_n} \tag{8}$$

where $\eta_{single_1}, \eta_{single_2}, \eta_{single_3}, \cdots, \eta_{single_n}$ refer to the attenuation function of a single-preparation module with different first gradient moments.

Assuming the simple case that the blood flows along the x-direction and ignoring the velocity dispersion along the x-direction, according to equation (6), the attenuation function of a single-preparation module would be

$$\eta_{single} = \cos\left(\gamma m_{1x} v_x\right)\ \mathrm{sinc}\left(\beta_y m_{1x}\Delta y\right)\ \mathrm{sinc}\left(\beta_z m_{1x}\Delta z\right) \tag{9}$$

where $\beta_y = \frac{\gamma}{2}\cdot\frac{\partial v_x}{\partial y}$, $\beta_z = \frac{\gamma}{2}\cdot\frac{\partial v_x}{\partial z}$.

If we assume the case that the velocity dispersion is proportional to velocity (Poiseuille flow, $\frac{\partial v_x}{\partial y} = k_y v_x$ and $\frac{\partial v_x}{\partial z} = k_z v_x$),

$$\eta_{single} = \cos\left(\gamma m_{1x} v_x\right) \operatorname{sinc}\left(\frac{\gamma m_{1x} \Delta y k_y}{2} v_x\right) \operatorname{sinc}\left(\frac{\gamma m_{1x} \Delta z k_z}{2} v_x\right) \quad (10)$$

where k_y and k_z are the ratio of velocity dispersion to velocity in y and z directions.

For demonstration purposes, we choose typical values of $m_{1x} = 0.3\ \mu\text{Ts}^2/\text{m}$ and $\Delta y = \Delta z = 1.4$ mm. The gyromagnetic ratio of the proton is γ=2.68 rad$\cdot 10^8/(\text{s}\cdot\text{T})$. Fig. 3 shows the simulated signal magnitude (in the dark-artery-vein image) as a function of blood flow velocity when the dispersion is small ($k_y = k_z = 100\,\text{m}^{-1}$), medium ($k_y = k_z = 200\,\text{m}^{-1}$) and large ($k_y = k_z = 300\text{m}^{-1}$). Substantial oscillations can be observed in the single flow preparation result, especially when the dispersion is small. For the double- or triple-preparation, these oscillations are reduced, and signal suppression is more consistent.

METHODS

Human studies were approved by the local research ethics committee, and all participants gave informed consent. Ten healthy volunteers (mean age 26 years, range 23–44 years; M/F = 6:4) and 13 patients (mean age 61 years, range 18–78 years; M/F = 11:2) with acute peripheral DVTs (in the femoral vein and/or proximal popliteal vein) diagnosed using ultrasound and no previous history of venous thrombosis or contraindications for MRI were recruited. Images of the lower legs were acquired in supine orientation using a 1.5 T scanner (Signa HDx, GE Healthcare, Waukesha, WI) and an eight-channel cardiac-array coil.

Before the NCE-MRV sequence, the flow velocity profiles were firstly measured using axial 2D cine phase-contrast (PC) imaging (echo time (TE) 3.5 ms; repetition time (TR) 6.9 ms; flip angle 30°; acquired matrix 256×128; field of view (FOV) 32×16 cm^2; slice thickness 5 mm; ***venc*** 50-70 cm/s; 100 cardiac phases (retrospective gating)). The ADVANCE-MRV sequence was used to acquire velocity- and acceleration-sensitised acquisitions in a coronal oblique orientation so that the flow was in-plane. The imaging parameters were: TE 1.7 ms; TR 3.7 ms; flip angle 65°; acquired matrix 256×256 or 288×288; number of slices 16 or 28; FOV 35–40 cm; slice thickness 2.4 mm. The cardiac trigger delay time was chosen to place the flow-sensitisation module at approximately peak arterial flow, as determined by the PC measurements. Each plane of k-space (k_x-k_y) was acquired over two shots. For the volume with 16 slices, the acquisition time was 32 heartbeats per volume. Table 1 shows the parameters of different sequence configurations, including $\mathbf{m_1}$, $\mathbf{m_2}$, total acquisition numbers, total acquisition time in heartbeats

and SARs. When using more preparation modules, the TR will be extended to offset the increase of SAR. Therefore, the SARs of different sequences are kept in a similar value in this study.

Parallel imaging (ASSET) was used with an acceleration factor of two. The reconstructed resolution was increased by a factor of two in all three directions using zero-fill interpolation. For each dataset, subtraction angiograms were generated automatically by subtracting the dark-artery image from the corresponding dark-artery and vein image. Maximum intensity projections (MIPs) were then produced from the subtracted datasets.

MR-DTI was performed only in the patient group in the coronal orientation, using a 3D inversion-prepared fast gradient-echo acquisition with a water-selective excitation (31). The imaging parameters were: inversion time (TI) 340 ms; TE 6.3 ms; TR 12.2 ms; flip angle 25°; acquired matrix 320×288×96; FOV 40×40 cm^2; slice thickness 2 mm; 320 ms delay after each shot. Parallel imaging (ASSET) was used with an acceleration factor of two. Zero-filling interpolation was used to increase the reconstructed volume size to 512×512×96. These parameters were chosen to optimise the relative enhancement of short-T_1 substances and suppress the signal from blood, based on simulations (31).

Evaluation of the impact of flow dispersion on venous signals

To assess the variation of blood signals with the $\mathbf{m_1}$ values of motion-sensitised gradients, the single-preparation scans were performed with 21 evenly-spaced $\mathbf{m_1}$ values, from 0–2.0 $\mu Ts^2/m$ in one representative healthy subject. Regions of interest (ROIs) were drawn on the original (unsubtracted) velocity-sensitised images. Representative deep vein segments were chosen from distal femoral vein in the lower thigh, where signal void artefacts can be observed.

Validation of the signal attenuation model

Multiple-slice axial 2D cine PC measurements were performed on a healthy volunteer to validate the predictions of the signal attenuation model (echo time (TE) 3.5 ms; repetition time (TR) 6.9 ms; flip angle 30°; acquired matrix 384×192; field of view (FOV) 40×20 cm^2; slice thickness 8 mm; ***venc*** 13 cm/s; 100 cardiac phases (retrospective gating)). Six representative slices were selected based on the MIP of initial ADVANCE-MRA images, which involve the regions where signal void artefacts appear. Velocity and velocity dispersion maps were calculated for the selected six slices. The velocity map shows the mean velocity of each pixel of the 100 cardiac phases. The velocity dispersion of a pixel is calculated by the sum-of-squares of its horizontal gradient and vertical gradient on the velocity map.

Evaluation of the multiple-acquisition and multiple-preparation methods on healthy volunteers

The quantitative assessment was performed on the datasets from ten healthy volunteers. The number of acquisitions or preparations utilised in this study were two (double-acquisition, double-preparation) or three (triple-acquisition, triple-preparation). Velocity-sensitised datasets were acquired five times with $\mathbf{m_1}$ for the first preparation of 150, 300, 600, 1200 and 2400 nTs^2/m respectively. The $\mathbf{m_1}$ for the second and third preparations were half and one-fourth of the $\mathbf{m_1}$ of first preparations for each acquisition. The $\mathbf{m_2}$ for acceleration-sensitised preparation module was 2.74 nTs^3/m in this study, which was chosen according to the evaluation in our previous study (24). The total acquisition time was 192 heartbeats for the volume with 16 slices or 336 heartbeats for the volume with 28 slices.

ROIs were drawn for the lumen regions with signal void artefacts on individual subtracted images from all ten healthy volunteers. Statistical analyses include normalized signal intensity, signal spatial variation ratio and ratio of signal variation with $\mathbf{m_1}$ values. The normalized signal intensity shows the signal intensity level, which is the mean signal intensity normalized by using the images of the initial sequence (single-preparation and single-acquisition) as the reference. The signal spatial variation ratio is the ratio of the standard deviation (SD) of pixel intensities in each ROI to their mean value, which reflects the signal uniformity. The ratio of signal variation with $\mathbf{m_1}$ values is the SD of mean signal intensities from images with different $\mathbf{m_1}$ values, divided by their mean value. It shows the dependence of the signal oscillation with varying ***venc***, which is expected to relate to the variation with varying flow velocity. The mean value of measurements for all ROIs on each volunteer was calculated. Measurements from the following ADVANCE-MRV based sequences were compared using a Student's paired t-test: initial sequence (single-preparation and single-acquisition); double-preparation; triple-preparation; double-acquisition; and triple-acquisition. A $P < 0.05$ was considered to indicate statistical significance. The signal intensity frequency distribution histograms of different methods were also drawn based on the measurements from one selected volunteer.

In order to evaluate the effect of multiple preparation modules on static tissue signal and background signal suppression, muscle signal was measured on both pre-subtracted dark-artery-vein images and subtracted angiograms for different sequences.

Evaluation on patients

The ADVANCE-MRV technique with double-preparation and double-acquisition was selected and evaluated in 13 patients with ultrasound-proven above-knee acute DVTs. The $\mathbf{m_1}$ velocity-sensitised

modules were 600 and 300 nTs^2/m in the first acquisition, and 300 and 150 nTs^2/m in the second acquisition. The $\mathbf{m_2}$ of the acceleration-sensitised module was 2.74 nTs^3/m. The total acquisition time was 96 heartbeats. MR-DTI was also performed in all patients. ROIs were drawn for lumen regions without occlusion on individual subtracted images from all the patient data. The signal spatial variation ratio was calculated. An experienced radiologist reviewed the patient studies to examine if signal void artefacts were present and to define the extent and location of thrombus by comparison with MR-DTI images.

Simulations for the B_0/B_1 inhomogeneity effect

Motion-sensitised preparations have been reported to suffer signal loss caused by inherent T_2 decay and sensitivity to B_0 and B_1 inhomogeneity (29). This signal loss might be increased by using multiple-preparation modules. Therefore, we undertook numerical simulations, based on the Bloch equations, to compare residual magnetisation after single-, double- or triple-preparations at different B_0 off-resonance (ΔB_0) and relative B_1 scaling factor (rB_1) values. A T_1 of 1000 ms and a T_2 of 200 ms were used in the simulations. The delay between RF pulses was 4 ms, and the duration of a 90° pulse was 0.4 ms. The phase shifts caused by one single velocity-sensitised gradient and one single acceleration-sensitised gradient were both set to 0.25π.

RESULTS

Fig. 4 shows example velocity-sensitised vein images and the signal attenuation with increasing gradient moment (0–1.2 $\mu Ts^2/m$). A substantial oscillation can be seen in the single-preparation images (arrows) and diagram. Oscillations are reduced in double- and triple-preparation images. The double-preparation approach achieved the best overall blood suppression. The triple-preparation approach has a very small signal variation, but residual signal exists due to insufficient blood suppression.

The velocity and velocity dispersion map in the axial plane obtained by PC measurements are shown in Fig. 5. Fig. 5a is an oblique plane reformat of an ADVANCE-MRV showing the locations of the six selected slices. Two observations can be made by comparing the axial plane reformats of ADVANCE-MRV (Fig. 4b) with the corresponding velocity map (Fig. 4c) and velocity dispersion map (Fig. 4d). First, the signal void artefacts mainly appear in the centre of the lumen, where the velocity dispersion is low. Second, the signal void artefacts are more severe in the locations where the velocity is lower.

Fig. 6 shows example images of subtraction venograms acquired with the initial sequence (single-preparation and single-acquisition), and with the new double-preparation, triple-preparation, double-acquisition and triple-acquisition approaches, all displayed with the same window width and level. Signal

void artefacts in the venous lumen in the single-preparation images are greatly reduced by using multiple preparations or acquisitions. The triple-preparation image has a lower signal level although it has excellent signal uniformity. The multiple-acquisition shows the highest signal intensity.

The statistical analyses are shown in Fig. 7 for the initial sequence, multiple-preparation approaches and multiple-acquisition approaches. The ratio of signal variation with $\mathbf{m}_1$ values (Fig. 7c) is not measured for multiple-acquisition approaches, because multiple-acquisition approaches include fewer datasets than multiple-preparation approaches due to the combination of two or three datasets. The mean signal spatial variation ratios ± standard deviation were calculated to be 0.35±0.08, 0.28±0.06, 0.28±0.06, 0.25±0.06 and 0.24±0.06 for the initial, double-preparation, triple-preparation, double-acquisition and triple-acquisition approaches respectively (Fig. 7a). The normalized signal intensity was calculated to be 1.06±0.24, 0.75±0.17, 1.22±0.13 and 1.29±0.14 for the double-preparation, triple-preparation, double-acquisition and triple-acquisition approaches respectively (Fig. 7b). The mean ratios of signal variation with different $\mathbf{m}_1$ values ± standard deviation were 0.16±0.06, 0.11±0.05 and 0.09±0.04 for the initial, double-preparation and triple-preparation approaches respectively (Fig. 7c).

Compared with the initial sequence using a single-preparation and a single-acquisition, multiple-preparation and multiple-acquisition approaches all have significantly reduced signal spatial variation ratios, indicating the improvement of signal uniformity (paired t-test, $P < 0.05$). The ratios of signal variation with different $\mathbf{m}_1$ values of double-preparation and triple-preparation approaches are both significantly lower than the initial sequence ($P < 0.05$). Although the triple-preparation has small signal variations, it has the lowest normalized signal intensity among all the approaches. The multiple-acquisition approaches have both a high signal intensity level and a low spatial variation ratio. There is no significant difference between the performance of the double-acquisition approach and the triple-acquisition approach ($P >0.05$). Reviewing all the measurement parameters showed that the double-preparation method achieves the best results of the multiple-preparation methods. The best overall result is achieved by the multiple-acquisition methods, although this comes at the cost of increased acquisition time. These statistical analysis results all correspond to the observations in Fig. 6.

The muscle signal intensities on the dark-artery-vein images using single-preparation, double-preparation and triple-preparation modules were 426.3±104.4, 315.6±67.9 and 290.5±57.7 respectively, indicating a significant signal decay in static tissue caused by the additional preparation modules ($P<0.05$). The residual muscle signal intensities on the subtracted angiograms were not increased (27.2±9.2 for single-preparation, 25.6±1.3 for double-preparation and 22.3±0.76 for triple-preparation), which is because the acceleration-sensitised module has the same preparation time and thus the same signal decay.

The mean signal spatial variation ratio of ROIs from lumen regions without occlusion in patient data is 0.17±0.03. The uniformity of venous signal in patient images was evaluated by an experienced radiologist. No signal void artefacts in patent veins were found in DVT patient images. The femoral vein occlusion was identified in all cases on ADVANCE-MRV. Fig. 8 shows the ADVANCE-MRV and MR-DTI images from an example patient with DVT in the left femoral vein. Acute thrombus is depicted by hyperintense signal on MR-DTI. The distal occlusion of the femoral vein can be clearly seen on the MIP of ADVANCE-MRV, which was consistent with the thrombus locations determined by MR-DTI.

Fig. 9 shows simulated magnetisation responses at different ΔB_0 and rB_1 conditions for single-, double- and triple-preparation iMSDE. The residual magnetisation is reduced when using multiple-preparation modules, especially for triple-preparation. When $\Delta B_0=0$ and $rB_1=1$, the residual magnetizations are 0.92, 0.85 and 0.79 for single-, double- and triple-preparation in both velocity-sensitised and acceleration-sensitised modules. This overall signal drop reflects the intrinsic T_2 decay during the prolonged preparation time. All the three techniques have uniform magnetisation responses when ΔB_0 and rB_1 are in a limited range, indicating good immunity to $\Delta B_0/rB_1$ non-uniformity.

DISCUSSION

An NCE-MRV technique, based on velocity- and acceleration-sensitised preparation modules and image subtraction, has been developed and evaluated. An important requirement of vein imaging methods is a reasonably uniform signal in unobstructed veins. In this paper, we analysed the venous signal variation from the initial ADVANCE-MRV sequence and proposed two different strategies to improve venous signal uniformity.

The signal attenuation of the velocity-sensitised iMSDE module contains not only a decaying component (the sinc function) but also an oscillatory component (the $\cos$ function). The decaying component is the factor contributing to the blood-suppression effect of the iMSDE module. However, in cases of slow and uniform blood flow which may be found in the peripheral veins, the decaying component may fail to give complete signal suppression unless a very large $\mathbf{m}_1$ is used. However, such a large $\mathbf{m}_1$ can also suppress background signal in dark-blood images, or cause artefacts related to eddy currents or bulk motion, both of which lead to unwanted phase changes within the iMSDE modules. The oscillatory component, which has been neglected in some previous treatments of signal attenuation in motion-sensitised preparation modules (30,32), can offer an additional mechanism of (partial) signal suppression but is not robust over a range of flow velocities—this is the reason for the insufficient blood suppression and signal void artefacts investigated in this study. The influence of the oscillatory component is not obvious when the blood flow

is fast and large velocity dispersion exists, such as in arterial blood suppression. However, for venous blood suppression, the oscillatory component can be highly relevant in voxels with little velocity dispersion. In addition, the signal decay is related to not only the gradient strength of the preparation module and the velocity dispersion, but also on the voxel size. It can be speculated that the signal void issue would become increasingly important as imaging resolution is increased, because the intravoxel flow dispersion is reduced with smaller voxel sizes.

Peripheral venous flow can be considered as laminar flow in most cases. According to the Hagen-Poiseuille equation, velocity can be expressed as $v(r)=\frac{\Delta p}{4\eta L}\left(R^2-r^2\right)$, where $\frac{\Delta p}{L}$ is the pressure gradient along the vessel, η is the dynamic viscosity of blood, R is the pipe radius, and r is the distance to the centre of the vessel. Velocity dispersion can, therefore, be expressed as $\frac{dv}{dr}=-\frac{\Delta p}{2\eta l}r$ or $\frac{dv}{dr}=\frac{-2r}{R^2-r^2}v$. It can be seen that velocity dispersion is proportional to the velocity and hence, insufficient blood suppression mostly occurs in slow venous flow that has a small velocity dispersion. Voxels in the centre of lumen have the maximum velocity but minimum velocity dispersion, which would easily generate signal oscillation, resulting in signal void artefacts in subtracted images. These signal void artefacts in the lumen centre could be confused with occlusion and increase the chance of misdiagnosis. In comparison, voxels at the edge of lumen have the maximum velocity dispersion and rarely generate signal oscillation. These conclusions are consistent with the observations in Fig. 5.

Both multiple-preparation and multiple-acquisition methods can reduce the oscillations of venous signal and thus achieve more consistent blood suppression. Experimental results show that multiple-acquisition methods achieved the strongest signal intensity level, but they also prolonged the total acquisition time. The increase of the acquisition time and the combination of multiple datasets can also result in misregistration artefacts, that may require post-processing correction. Multiple-preparation methods improve blood suppression by adding two or three preparation modules together in one acquisition and thus do not increase the scan time for the protocols used in this paper. In all cases where non-uniformity was apparent, the addition of a second preparation module substantially improved the vein signal uniformity. Adding a third preparation module provided further uniformity improvements, but overall signal levels were reduced due to the intrinsic T_2 signal decay, increased eddy currents and increased sensitivity to B_0/B_1 non-uniformity on dark-blood images during the prolonged preparation time. Muscle signal measurement results showed a reduction of 31.8% in the pre-subtracted dark-artery-vein images. This signal decay can also be shown by numerical simulations based on the Bloch equations (Fig. 9).

Therefore, double-preparation was utilised for examinations of patients in this study as it offered a good compromise between optimising signal uniformity, signal intensity and scan time.

For examinations in patients, we used the sequence with double-preparation and double-acquisition to ensure venous signal with optimal intensity and uniformity. The signal spatial variation ratio in the patient data was 0.17±0.03. Since the initial sequence with single-preparation and single-acquisition was not obtained in the patients owing to the limited examination time, the quantitative measurements of patient data lack direct comparison with the initial approach. However, if we compare these values with the measurements from the healthy volunteers, the signal spatial variation ratio of the improved approach (0.17±0.03) can be considered as a very low value, since it is much lower than that of all the approaches on healthy volunteers, including the single-preparation sequence (0.35±0.08), multiple-preparation sequences (0.28±0.06 and 0.28±0.06) and multiple-acquisition sequences (0.25±0.06 and 0.24±0.06). In addition, no signal void artefacts in patent veins were observed in the patient images.

Our previous study has shown that for the ADVANCE-MRA technique, the arterial and venous signals are clearly separated over a wide range of $\mathbf{m_2}$ (2.62–26.2 nTs^3/m). Choosing large $\mathbf{m_2}$ values can suppress arterial signal more thoroughly but may impair venous signal. Considering it preferable to retain some arterial signal rather than impairing venous signal for venography, we chose a relatively small value of $\mathbf{m_2}$ (2.74 nTs^3/m) in this study. Benefiting from using multiple velocity-sensitised modules, $\mathbf{m_1}$ can also be chosen over a wide range. Experimental results show ADVANCE-MRA achieved good performance using $\mathbf{m_1}$ from 300 nTs^2/m to 2400 nTs^2/m.

One limitation of this study is that single-preparation and single-acquisition ADVANCE-MRV was not compared with the double-preparation and double-acquisition sequence in the patient study. Therefore, the potential improvements of the new strategies over the initial sequence in cases of slow flow in veins with occlusion was not evaluated. Secondly, the proposed NCE-MRV technique was only tested in femoral veins. Subtraction MRA with motion-sensitised preparation modules has been applied in other areas including calf (23), hand (33,34), foot (35) and thorax (36). Future work will evaluate the feasibility of this technique in other body areas. Additionally, other than multiple-preparation modules with different amplitudes, multiple-preparation modules with different gradient directions (34) will also be investigated, which would allow flow to be suppressed even in vessels with varying directions and may provide another mechanism for improving the poor signal suppression addressed in this work.

CONCLUSIONS

In conclusion, a non-exogenous contrast-enhanced MR venography technique has been developed and demonstrated in healthy volunteers and patients with known DVTs. The use of multiple preparations or multiple acquisitions substantially reduced the problem of intravascular signal void artefacts, providing uniform venous signal. The technique has the potential for improving the diagnostic performance of MR venography in the detection of lower limb DVTs which will require further patient studies to demonstrate.

ACKNOWLEDGEMENT

The authors would like to thank Trevor Baglin and the Department of Haematology, Addenbrooke's Hospital for their contribution in patient recruitment. The authors acknowledge the support of the Addenbrooke's Charitable Trust and the NIHR Cambridge Biomedical Research Centre. Hao Li acknowledges the China Scholarship Council and Cambridge Trust for fellowship support.

REFERENCE

1. Tan M, Van Rooden CJ, Westerbeek RE, Huisman M V. Diagnostic management of clinically suspected acute deep vein thrombosis. Br J Haematol. 2009;146:347–360
2. Katz DS, Hon M. Current DVT imaging. Tech Vasc Interv Radiol. 2004;7:55–62
3. Wells PS, Lensing AW, Davidson BL, Prins MH, Hirsh J. Accuracy of ultrasound for the diagnosis of deep venous thrombosis in asymptomatic patients after orthopedic surgery. A meta-analysis. Ann Intern Med. 1995;122:47–53.
4. Fraser JD, Anderson DR. Deep venous thrombosis: recent advances and optimal investigation with US. Radiology 1999;211:9–24.
5. Kanne JP, Lalani TA. Role of computed tomography and magnetic resonance imaging for deep venous thrombosis and pulmonary embolism. Circulation 2004;109:I15–I21.
6. Moody AR. Magnetic resonance direct thrombus imaging. J Thromb Haemost. 2003;1:1403–1409.
7. Treitl KM, Treitl M, Kooijman-Kurfuerst H, et al. Three-dimensional black-blood T1-weighted turbo spin-echo techniques for the diagnosis of deep vein thrombosis in comparison with contrast-enhanced magnetic resonance imaging: A pilot study. Invest. Radiol. 2015;50:401–408.
8. Yang Q, Duan J, Fan Z, et al. Early Detection and Quantification of Cerebral Venous Thrombosis by Magnetic Resonance Black-Blood Thrombus Imaging. Stroke 2016;47:404–409.

9. Xie G, Chen H, He X, et al. Black-blood thrombus imaging (BTI): a contrast-free cardiovascular magnetic resonance approach for the diagnosis of non-acute deep vein thrombosis. J. Cardiovasc. Magn. Reson. 2017;19:1–11.
10. Westerbeek RE, Van Rooden CJ, Tan M, et al. Magnetic resonance direct thrombus imaging of the evolution of acute deep vein thrombosis of the leg. J Thromb Haemost. 2008;6:1087–1092.
11. Mendichovszky IA, Priest AN, Bowden DJ, et al. Combined MR direct thrombus imaging and non-contrast magnetic resonance venography reveal the evolution of deep vein thrombosis: a feasibility study. Eur Radiol. 2017;27:2326–2332.
12. Marckmann P. Nephrogenic systemic fibrosis: suspected causative role of gadodiamide used for contrast-enhanced magnetic resonance imaging. J Am Soc Nephrol. 2006;17:2359–2362.
13. Kanda T, Ishii K, Kawaguchi H, Kitajima K, Takenaka D. High signal intensity in the dentate nucleus and globus pallidus on unenhanced T1-weighted MR images: relationship with increasing cumulative dose of a gadolinium-based contrast material. Radiology. 2014;270:834–841.
14. Kanda T, Osawa M, Oba H, et al. High signal intensity in dentate nucleus on unenhanced T1-weighted MR images: association with linear versus macrocyclic gadolinium chelate administration. Radiology. 2015;275:803–809.
15. Kanda T, Fukusato T, Matsuda M, et al. Gadolinium-based contrast agent accumulates in the brain even in subjects without severe renal dysfunction: evaluation of autopsy brain specimens with inductively coupled plasma mass spectroscopy. Radiology. 2015;276:228–232.
16. U.S. Food and Drug Administration. FDA warns that gadolinium-based contrast agents (GBCAs) are retained in the body; requires new class warnings. https://www.fda.gov/downloads/Drugs/DrugSafety/UCM589442.pdf. Published May 22, 2017.
17. European Medicines Agency. Gadolinium-containing contrast agents. EMA's final opinion confirms restrictions on use of linear gadolinium agents in body scans. http://www.ema.europa.eu/docs/en_GB/document_library/Referrals_document/gadolinium_contrast_agents_31/Opinion_provided_by_Committee_for_Medicinal_Products_for_Human_Use/WC500231824.pdf. Published July 21, 2017.
18. Evans AJ, Sostoman HD, Knelson MH, et al. Detection of deep venous thrombosis: prospective comparison of MR imaging with contrast venography. Am J Roentgenol 1993;161:131–139.
19. Koktzoglou I, Lim RP, Oisin F, Edelman RR. Non-contrast enhanced MRA. In: Syed M. Basic principles of cardiovascular MRI: physics and imaging technique. ed. Cham: Springer; 2015:297–314.
20. Cantwell CP, Cradock A, Bruzzi J, Fitzpatrick P, Eustace S, Murray JG. MR venography with true fast imaging with steady-state precession for suspected lower-limb deep vein thrombosis. J Vasc

Interv Radiol 2006;17:1763–1769.

21. Shin T, Kligerman SJ, Crawford RS, Rajagopalan S, Gullapalli RP. Noncontrast-enhanced peripheral venography using velocity-selective magnetization preparation and transient balanced SSFP. Magn. Reson. Med. 2016;75:653–664.
22. Ono A,Murase K, Taniguchi T, Shibutani O, Takata S, Kobashi Y, Miyazaki M. Deep vein thrombosis using non-contrast-enhanced MR venography with electrocardiographically gated three-dimensional half-Fourier FSE: preliminary experience. Magn ResonMed 2009;61:907–917.
23. Priest AN, Graves MJ, Lomas DJ. Non-contrast-enhanced vascular magnetic resonance imaging using flow-dependent preparation with subtraction. Magn Reson Med. 2012;67:628–637.
24. Priest AN, Taviani V, Graves MJ, Lomas DJ. Improved artery-vein separation with acceleration-dependent preparation for non-contrast-enhanced magnetic resonance angiography. Magn Reson Med. 2014;72:699–706.
25. Fan Z, Sheehan J, Bi X, Liu X, Carr J, Li D. 3D noncontrast MR angiography of the distal lower extremities using flow-sensitive dephasing (FSD)-prepared balanced SSFP. Magn Reson Med. 2009;62:1523–1532.
26. Priest AN, Graves MJ, Lomas DJ. MR Leg Venography : improved methodology & impact of subject positioning. In Proceedings of the 19th Annual Meeting of ISMRM, Montreal, Canada, 2011. p. 1289.
27. Priest AN, Graves MJ, Lomas DJ. Non-contrast-enhanced vein imaging in the deep veins: impact of velocity patterns and improved image quality. In Proceedings of the 20th Annual Meeting of ISMRM, Melbourne, Australia, 2012. p. 1210.
28. Priest AN, Joubert I, Hilborne S, et al. Non-contrast-enhanced imaging of lower limb veins: improved imaging using multiple flow preparations. In Proceedings of the 21st Annual Meeting of ISMRM, Salt Lake City, Utah, USA, 2013. p. 1287.
29. Wang J, Yarnykh VL, Yuan C. Enhanced image quality in black-blood MRI using the improved motion-sensitized driven-equilibrium (iMSDE) sequence. J Magn Reson Imaging. 2010;31:1256–1263.
30. Wang J, Yarnykh VL, Hatsukami T, Chu B, Balu N, Yuan C. Improved suppression of plaque-mimicking artifacts in black-blood carotid atherosclerosis imaging using a multislice motion-sensitized driven-equilibrium (MSDE) turbo spin-echo (TSE) sequence. Magn Reson Med. 2007;58:973–981.
31. Priest AN, Joubert I, Hilborne S, et al. MR direct thrombus imaging with optimised signal and improved lipid suppression. In Proceedings of the 21st Annual Meeting of ISMRM, Salt Lake City, Utah, USA, 2013. p. 1280.
32. Fan Z, Zhou X, Bi X, Dharmakumar R, Carr JC, Li D. Determination of the optimal first-order

gradient moment for flow-sensitive dephasing magnetization-prepared 3d noncontrast MR angiography. 2011;972:964–972.

33. Sheehan JJ, Fan Z, Davarpanah AH, et al. Nonenhanced MR angiography of the hand with flow-sensitive dephasing-prepared balanced SSFP sequence: initial experience with systemic sclerosis. Radiology. 2011;259:248–256.
34. Fan Z, Hodnett PA, Davarpanah AH, et al., Noncontrast MR Angiography of the Hand: Improved Arterial Conspicuity by Multi-Directional Flow-Sensitive Dephasing Magnetization Preparation in 3D Balanced SSFP Imaging. Invest. Radiol. 2011;46:515–523.
35. Liu X, Fan Z, Zhang N, et al. Unenhanced MR angiography of the foot: initial experience of using flow-sensitive dephasing-prepared steady-state free precession in patients with diabetes. Radiology. 2014;272:885–894.
36. Priest AN, Low G, Graves MJ, Lomas DJ. Non-contrast-enhanced MR angiography of the thoracic central veins. In Proceedings of the 22nd Annual Meeting of ISMRM, Milan, Italy, 2014. p. 2513.

Figures

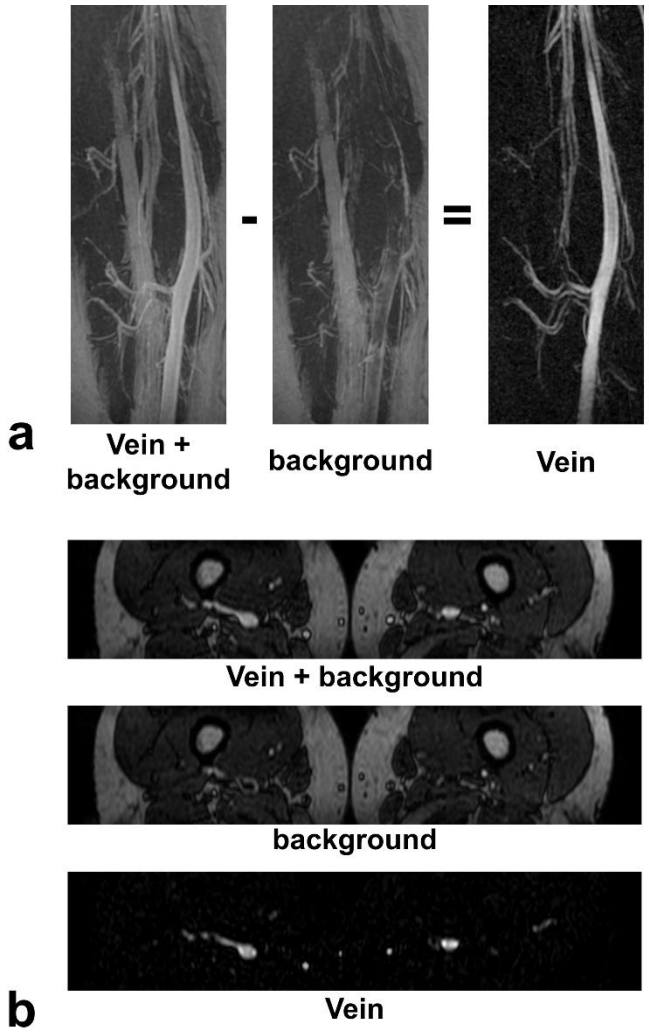

FIG. 1. Subtraction scheme of the ADVANCE-MRV method. The venous image is formed by subtracting an image with all vessels suppressed (obtained using velocity-sensitive preparation) from an image with arteries suppressed only (obtained using acceleration-sensitive preparation). **a:** Coronal maximum intensity projections (MIPs); **b:** Axial single slices.

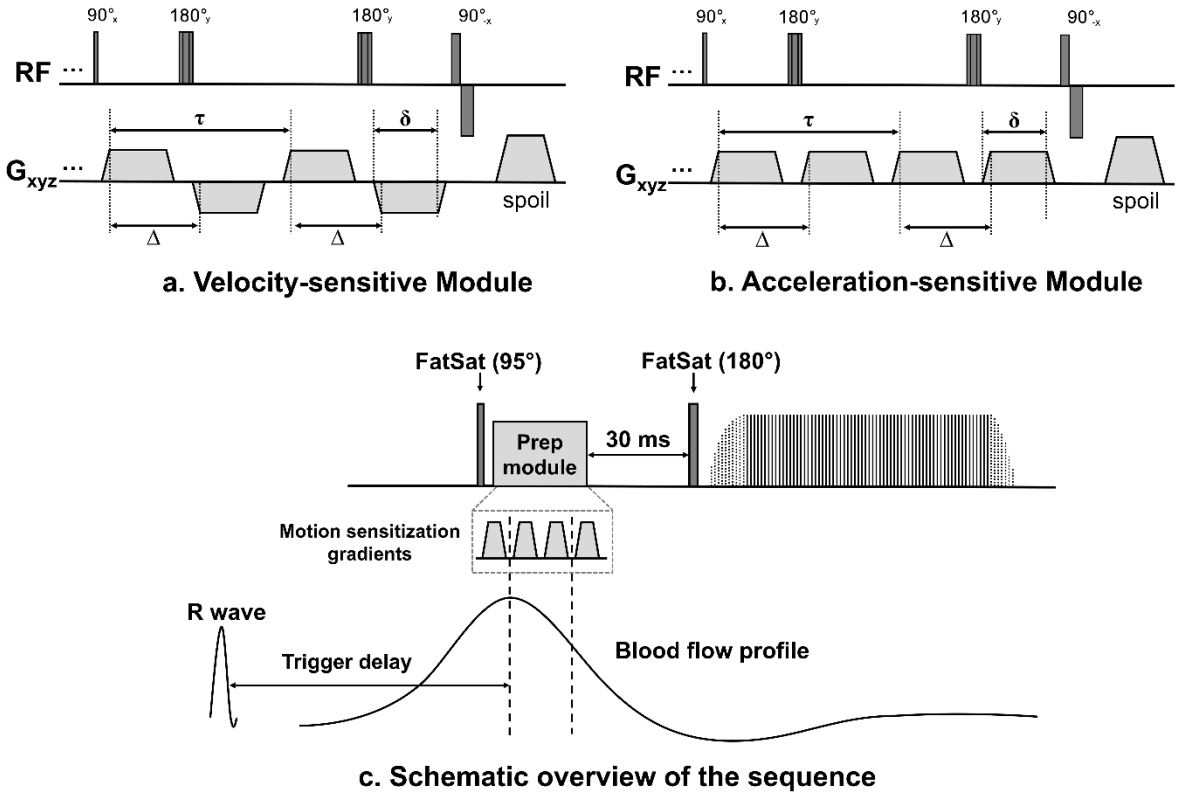

FIG. 2. Schematic diagram of the ADVANCE-MRV pulse sequence. **a:** Detail of the velocity-sensitive iMSDE module; **b:** Detail of the acceleration-sensitive sensitised iMSDE module; **c:** Schematic overview of the ADVANCE-MRV sequence. The mid-point between the first and second gradients of the preparation module is aligned with the peak systolic flow.

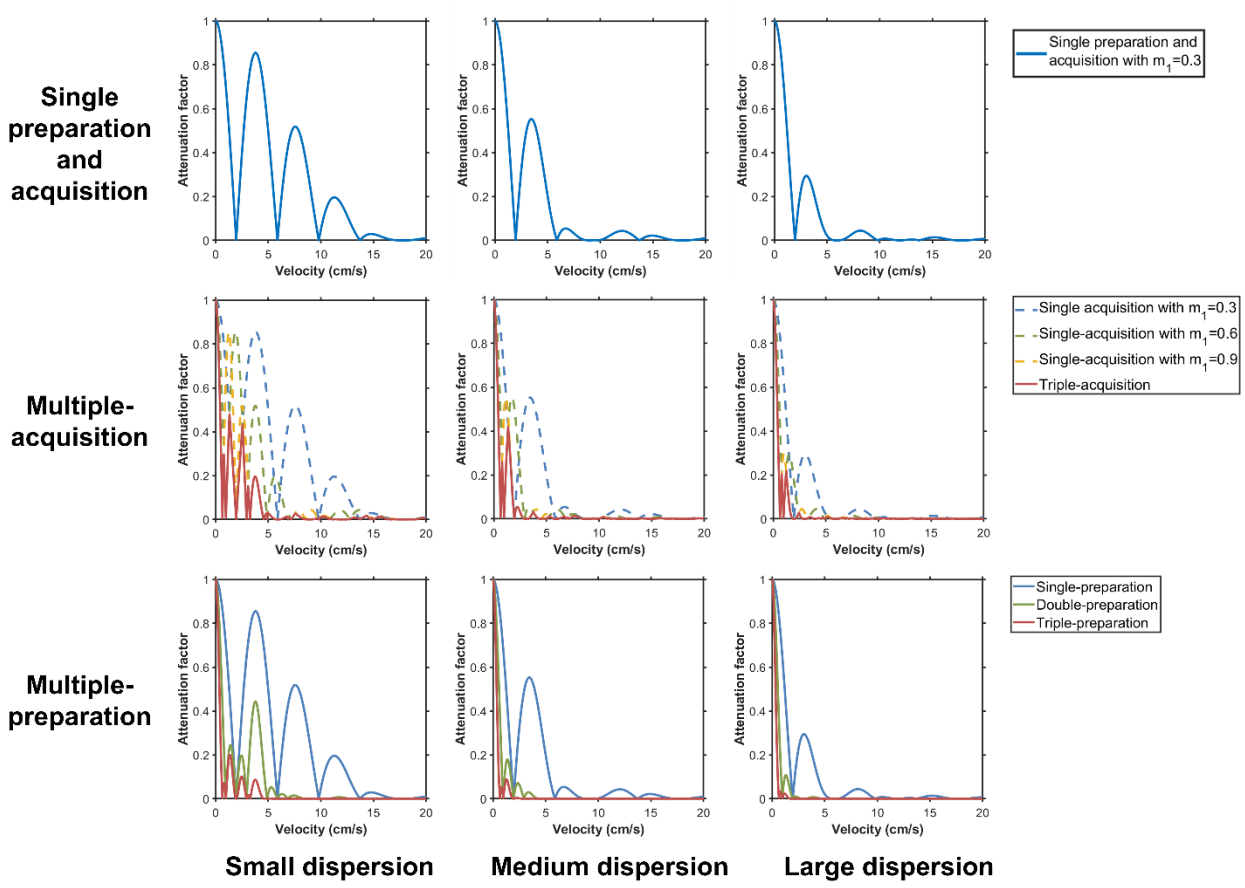

FIG. 3. Simulated signal profiles of two strategies as a function of velocity with small dispersion ($k_y = k_z = 100\,\mathrm{m}^{-1}$), medium dispersion ($k_y = k_z = 200\,\mathrm{m}^{-1}$) and large dispersion ($k_y = k_z = 300\mathrm{m}^{-1}$). Signal oscillations shown in the single-preparation method can be largely reduced in both multiple-acquisition and multiple-preparation methods, especially when the flow velocity dispersion is small.

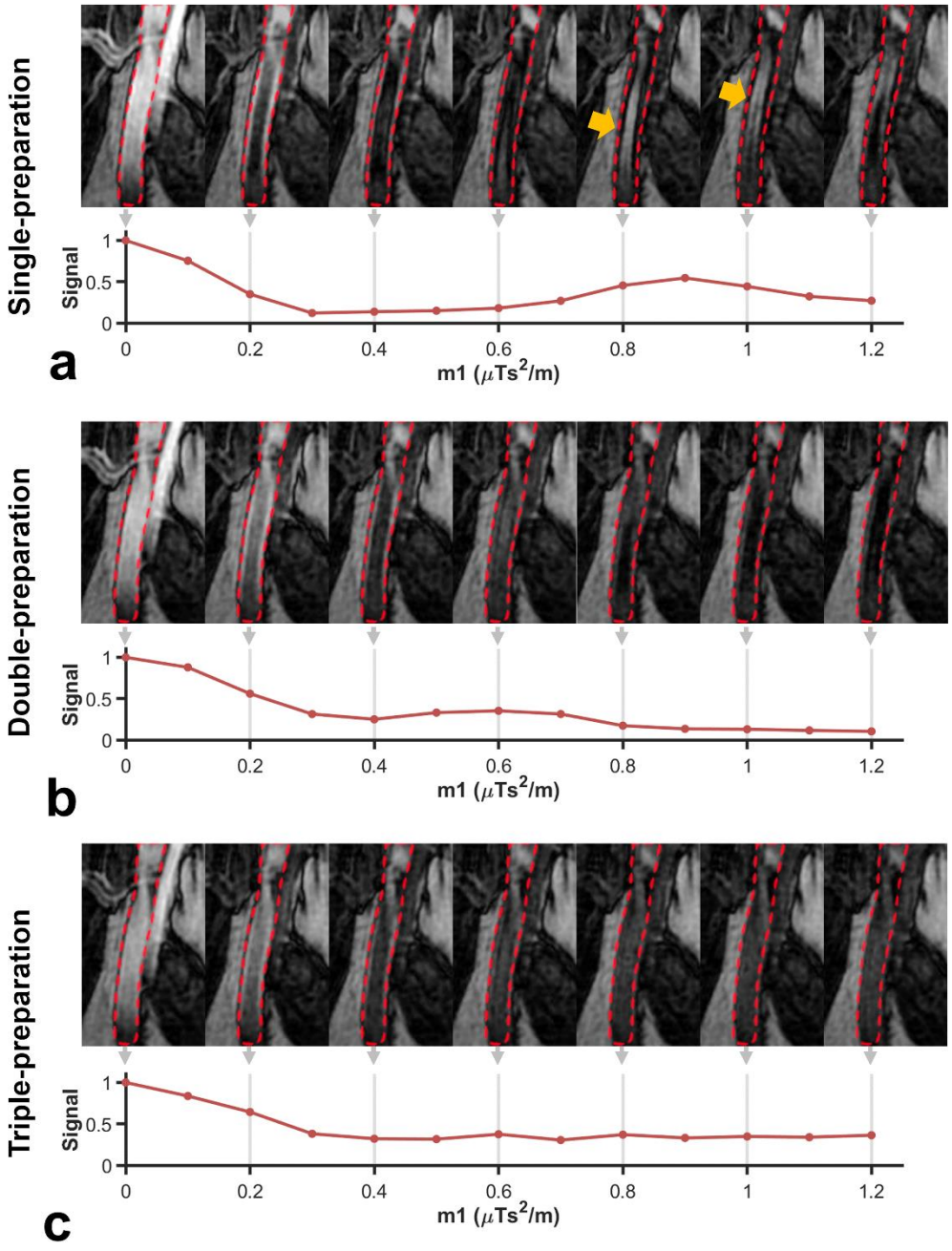

FIG. 4. Venous signal variation with increasing gradient moment (0–1.2 μTs^2/m) for single-preparation (**a**), double-preparation (**b**) and triple-preparation (**c**). The above velocity-sensitised (pre-subtraction) images show an outlined vein (and adjacent artery). The signal attenuation graph below shows the corresponding normalised mean signal intensity of the outlined vein in each phase. The $\mathbf{m_1}$ values of double-preparation method refer to the smaller $\mathbf{m_1}$ values of the two preparation modules. The yellow arrows indicate a venous signal oscillation in single-preparation images, which is suppressed in both double- and triple-preparation images.

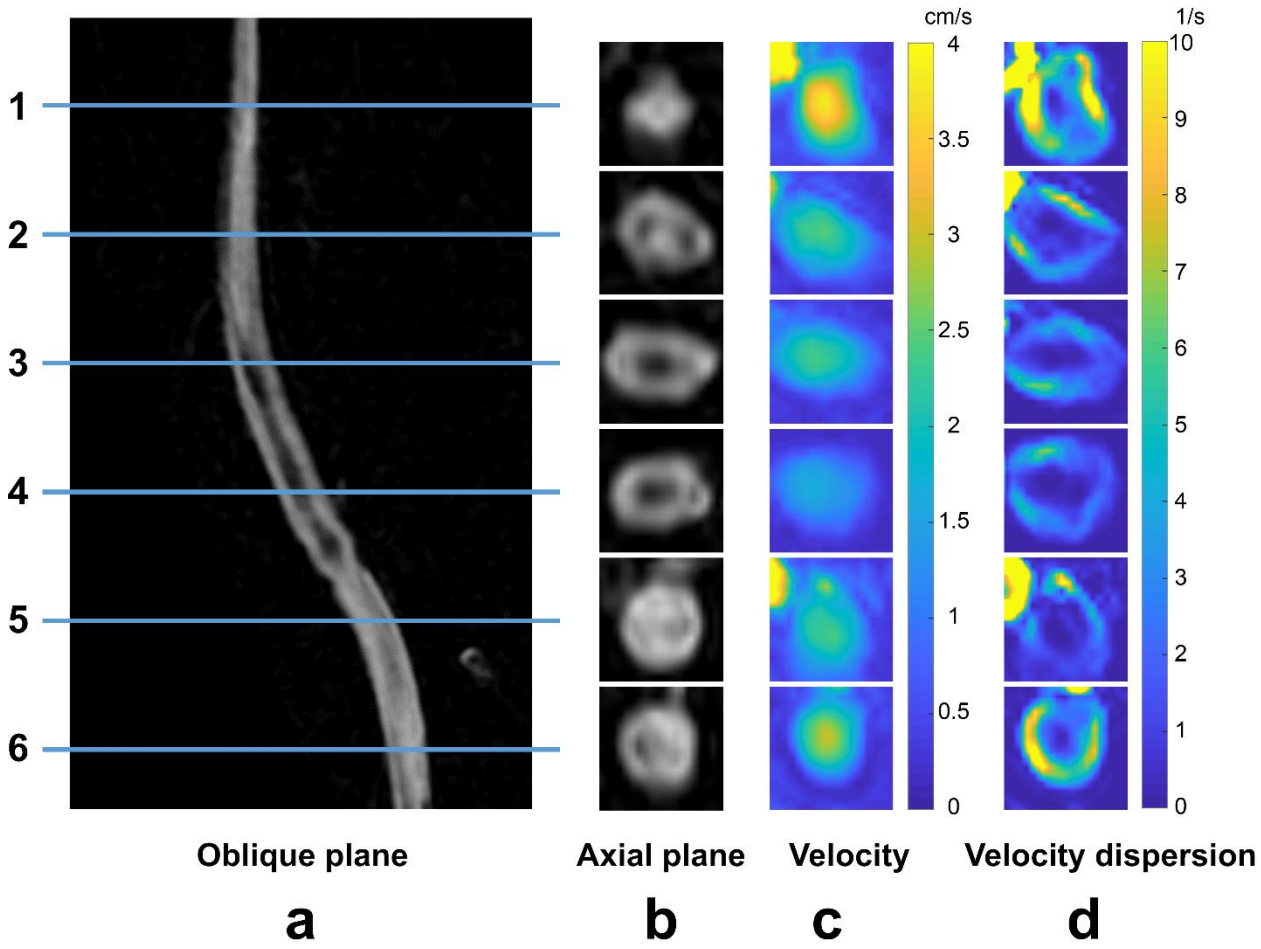

FIG. 5. Velocity and velocity dispersion maps on representative slices from a healthy volunteer. **a:** An oblique plane reformat of ADVANCE-MRV. 2D PC-MRA was acquired at the six locations shown. **b:** The axial plane reformats of ADVANCE-MRV corresponding to the selected slices. **c:** Velocity map in the axial plane corresponding to selected slices. **d:** Velocity dispersion map in axial plane corresponding to selected slices.

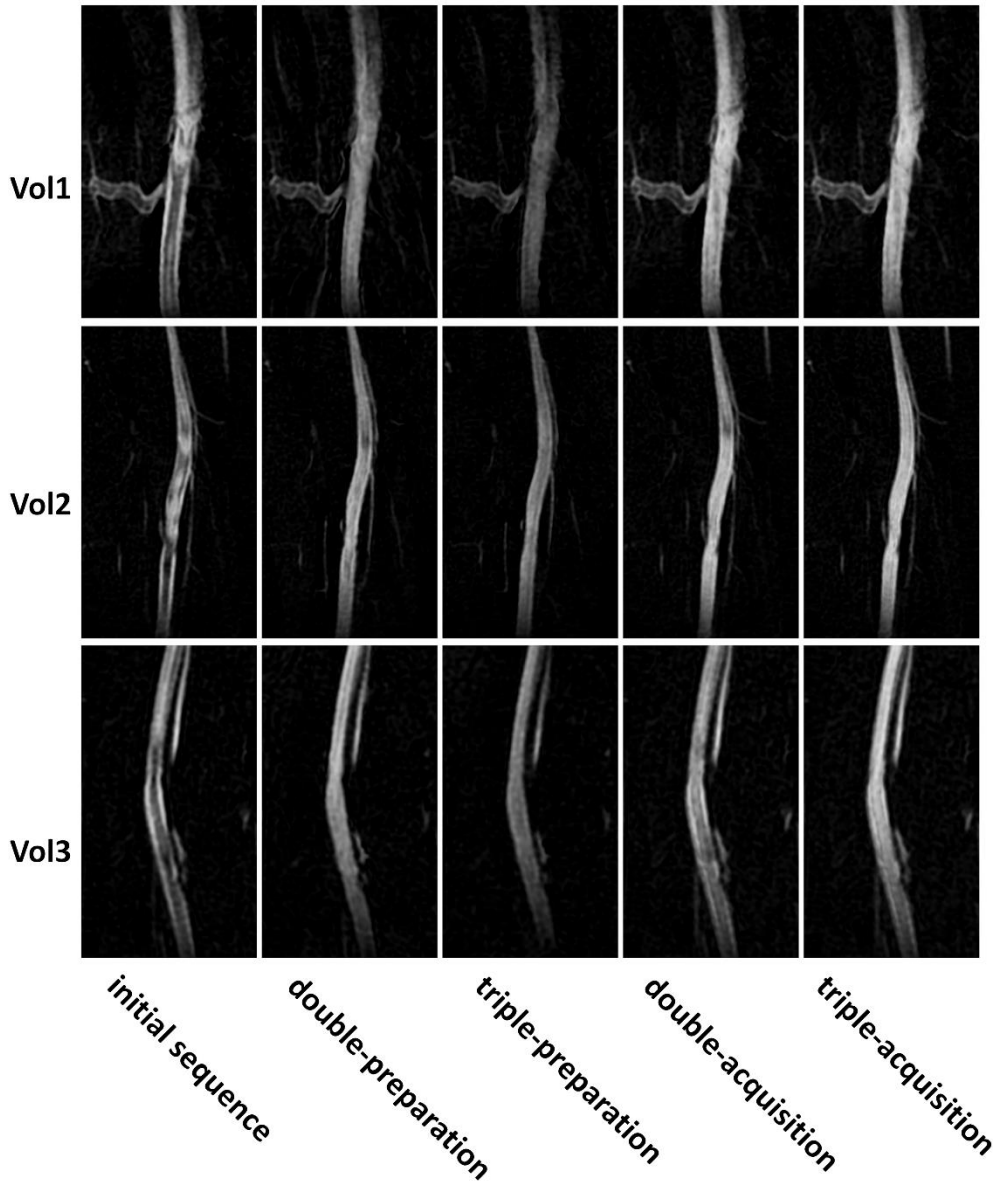

FIG. 6. Example matching subtraction angiograms from three volunteers showing the signal void artefacts in the initial sequence (single-preparation and single-acquisition) and improvement in sequences with multiple preparations or multiple acquisitions. The images are shown as curved-plane reformats through the vessel centre-line.

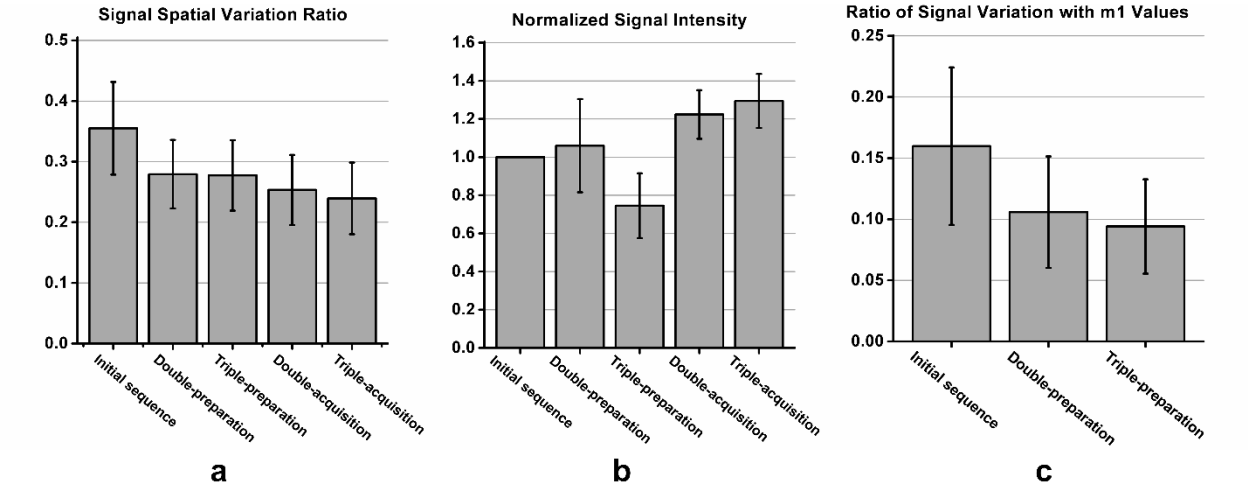

FIG. 7. Histograms of **a:** signal spatial variation ratio **b:** normalized signal intensity and **c:** ratio of signal variations with $\mathbf{m_1}$ values. Error bars represent one standard deviation over the set of subjects.

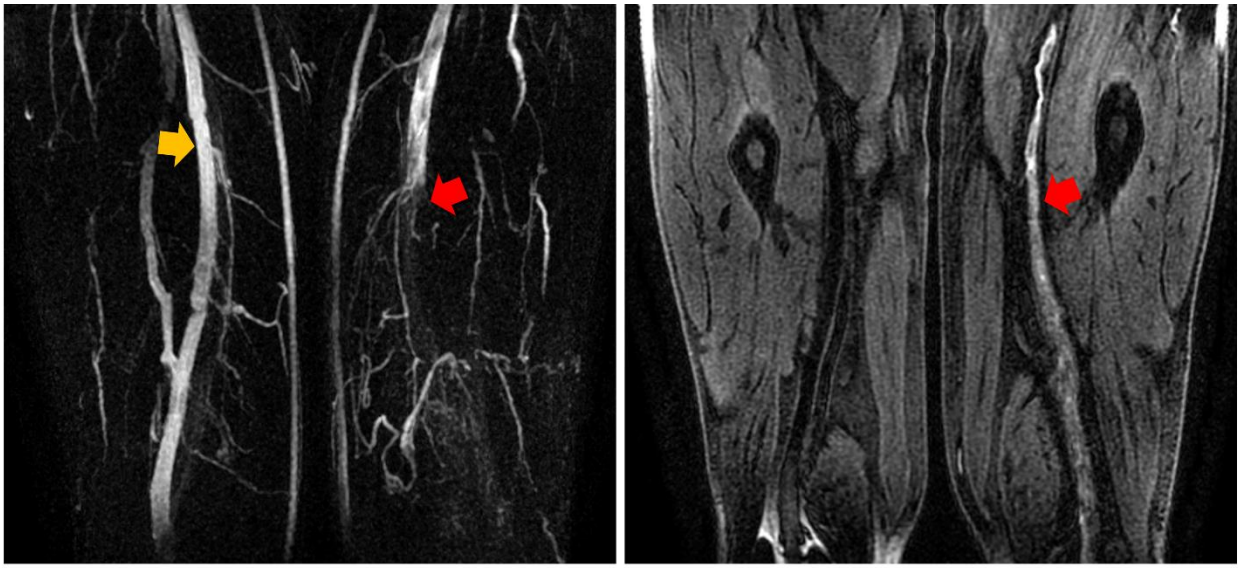

FIG. 8. **a:** The MIP of ADVANCE-MRV (double-preparation and double-acquisition) from a patient with DVT, showing occlusion of the left femoral vein by thrombus (red arrow) and uniform signal in the non-occluded vessel (yellow arrow). **b:** The corresponding MR-DTI image (curved-plane reformat), showing thrombus in the left femoral vein (red arrow).

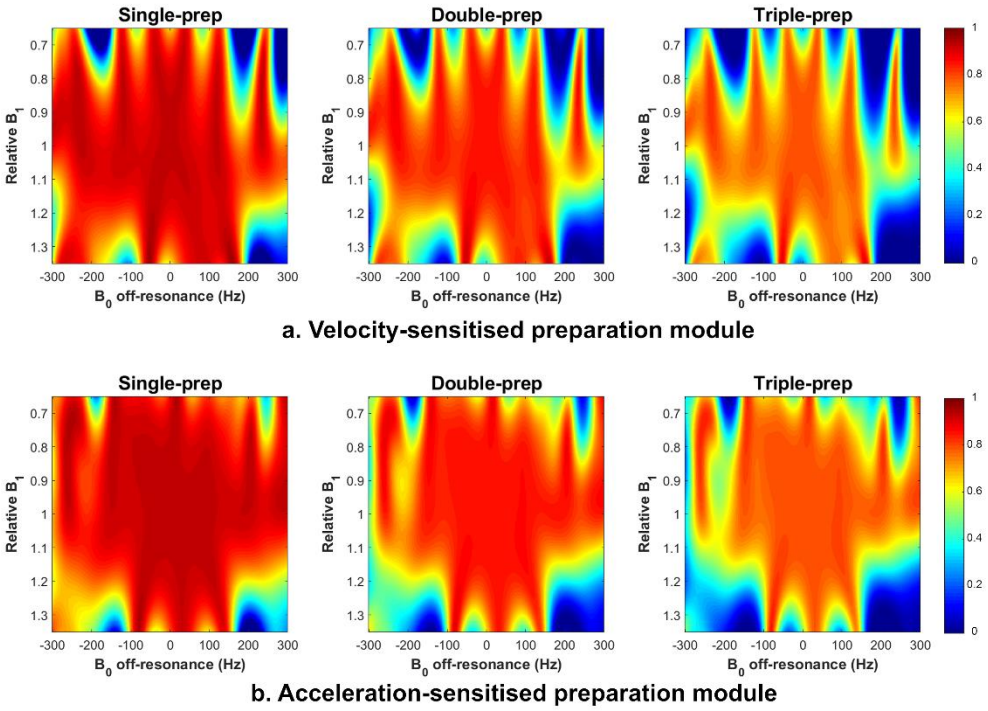

FIG. 9. Bloch equation-based simulations to evaluate the magnetisation responses for different velocity-sensitised (**a**) and acceleration-sensitised (**b**) preparation modules at different ΔB_0 and rB_1 values. T_1=1000 ms, T_2=200 ms. The residual magnetisation is reduced when using multiple-preparation modules, especially for triple-preparation. All these techniques have uniform magnetisation responses when ΔB_0 and rB_1 are in a limited range.

List of tables:

TABLE 1. Difference in parameters between the different sequence configurations

Strategies	$\mathbf{m_1}$ (nTs^2/m)				$\mathbf{m_2}$ (nTs^3/m)	Acquisition number	Scan time (heartbeats)	SAR (W/kg)
	Module 1	Module 2	Module 3	Module 4				
single-preparation, single-acquisition	600	-	-	-	2.74	2	64	1.61
double-preparation, single-acquisition	600	300	-	-	2.74	2	64	1.59
triple-preparation, single-acquisition	600	300	150	-	2.74	2	64	1.56
double-acquisition, single-preparation	600	300	-	-	2.74	3	96	1.61
triple-acquisition, single-preparation	600	300	150	-	2.74	4	128	1.61
double-preparation, double-acquisition	600	300	300	150	2.74	3	96	1.63